BROOKHAVEN
NATIONAL LABORATORY

BNL-75393-2006-IR

Polyphenylenesulfied/Montomorillonite Clay Nanocomposite Coatings: Their Efficacy in Protecting Steel Against Corrosion

Toshifumi Sugama
Energy Science & Technology Department
Brookhaven National Laboratory
Upton, NY 11973-5000

Keith Gawlik
National Renewable Energy Laboratory
1617 Cole Boulevard
Golden, CO 80401

June 2005

DISCLAIMER

Abstract

Nanoscale montomorillonite (MMT) clay fillers became dispersed in a polyphenylenesulfied (PPS) matrix through the processes of octadecylamine (ODA) intercalation → molten PPS co-intercalation → exfoliation. Cooling this molten exfoliated material led to the formation of a PPS/MMT nanocomposite. The MMT nanofiller conferred three advanced properties on the semi-crystalline PPS: First, it raised its melting point by nearly 40°C to 290°C; second, it increased its crystallization energy, implying that an excellent adherence of the nanofillers' surfaces to PPS in terms of a good interfacial bond; and, third, it abated the degree of its hydrothermal oxidation due to sulfide → sulfite linkage transformations. When this advanced PPS nanocomposite was used as a corrosion-preventing coating for carbon steel in a simulated geothermal environment at 300°C, a coating of ~ 150 μm thickness adequately protected the steel against hot brine-caused corrosion. In contrast, an MMT-free PPS coating of similar thickness was not nearly as effective in mitigating corrosion as was the nanocompsite; in fact, the uptake of corrosive ionic electrolyte by the unmodified coating increased with an extending exposure time.

Keywords: Coatings; Corrosion and oxidation; Nanocomposites; Polymers; Geothermal

1. Introduction

Polyphenylenesulfide (PPS)-based composite materials containing silicon carbide (SiC) and carbon fiber as thermal conductors exhibit a high potential as thermally conductive, anti-corrosion and-fouling liners for carbon steel heat exchanger tubes at geothermal binary-cycle power plants. In fact, our ~ 27 month field-validation test at the power plant operating at a brine temperature of 160°C gave a very promising result; the liner retained its integrity, including excellent hydrothermal stability, protection of the underlying tubes against corrosion, and minimization of silicate- and silica-related scale deposits [1-2]. This information strongly suggested that this liner would satisfactorily withstand such a harsh geothermal environment at 160°C.

Our most recent field exposure test at the power plant was devoted to investigating the stability of the liner exposed to brine at the upgraded temperature of 200°C. For this, we exposed PPS composite-coated carbon steel coupons to injected geothermal fluid at 200°C for four weeks. Post-test analyses showed that the composite coating adequately protected the carbon steel against corrosion as it did at 160°C. More importantly, the adherence of silicate and silica scales to the coating was very weak, so that the scale layers could readily be scoured off from its surfaces using the conventional method of cleaning by hydroblasing at low hydrostatic pressure [3]. In contrast, the surfaces of the stainless steel (SS), which is commonly used for the metal components in the power plants, were vulnerable to reaction with these scales. The major factor in this undesirable happening was the formation of passive oxide layers, the corrosion resistant barrier, at the outermost surface sites of the SS. The oxide layers favorably reacted with minerals in the geothermal fluid during the exposure, so promoting the deposition of scales and the development of a strong adherence to them. Thus, despite using high-pressure hydroblasting, some scales were difficult to remove completely from the SS's surface.

Since the melting temperature of PPS is around 250°C, it is reasonable to assume that this composite is able to withstand the brine temperatures up to 200°C. Thus, our next biggest challenge was to apply this composite to the carbon steel plant components intended to be used at a higher brine temperatures above 250°C. We previously studied the hydrothermal stability of this composite coating autoclaved at 250°C [4]. The results

revealed that the PPS underwent a hot brine-induced oxidation, thereby changing its molecular sulfide bridges to sulfone ones. This alteration allowed corrosive ionic species to permeate gradually through the oxidized PPS with increasing exposure time. Undoubtedly, increasing the melting temperature of PPS is an inevitable next step, if its potential application is targeted towards protecting carbon steel components at $\geq 250°C$ against corrosion and scale deposition. One specific area of application in the geothermal plants is the production wellhead, consisting of a flow line and tee, valve, and casing head, that encounter a very harsh environment with a flow velocity of ~ 3 m/sec of brine at 250°C. At present, a titanium alloy-based metal is commonly used in assembling the wellhead. Hence, if this could be replaced by an inexpensive carbon steel wellhead coated with a cost-effective, anti-corrosion and -fouling PPS composite, we believe that capital expenditure would fall considerably.

In trying to enhance the melting point of PPS, our particular interest was in adapting the polymer/clay nanocomposite technology by using montomorillonite (MMT) clay as the alternative nanoscale filler. As well documented by many investigators [5-10], MMT consists of one alumina octahedral sheet sandwiched between two silica tetrahedral sheets in which the fundamental unit is ~ a one nanometer (nm) thick, and has an approximately one hundred to several hundred nm long planar structure. Importantly, the basal space and gallery of ~ 1.1 nm between the alumina and silica sheets includes various cation-exchangeable Na^+, K^+, Li^+, or Ca^{2+} ions. These ions can easily exchanging with organic alkyl amine cations. Thus, the initial step of preparing a nanoscale MMT filler is the intercalation of such organic macromolecule ion exchangers containing a long alkyl chain linked to ionic amine into the gallery, thereby substantially expanding the gallery. Then, these spaces in the gallery expanded by the intercalated alkyl amine macromolecules lead to promoting the co-intercalation of polymers during curing, followed by the exfoliation of individual silicate platelets of ~ one nm thick. Accordingly, the aspect ratio of the exfoliated MMT nanofiller in the polymer matrix is very large. As a result, such dispersion of exfoliated MMT nanofillers significantly improved some properties of the polymer including mechanical properties, thermal stability, and fire retardation [11-14].

Based upon this information, the emphasis of the present study was directed towards investigating the usefulness of chemically treated MMT nanofillers in enhancing the melting point of PPS. Also, it included defining the characteristics of MMT-filled PPS nanocomposite material as a corrosion-preventing coating for carbon steel in a CO_2-laden brine at 300°C.

2. Experimental Procedures

Materials

Montomorillonite (MMT) filler was obtained from Aldrich Chemical Inc; it included cation-exchangeable sodium, Na. The same company also provided the octadecylamine [$CH_3(CH_2)_{17}NH_2$, ODA] used as a pretreatment reagent for the MMT. The ODA was intercalated into the basal gallery of MMT in the following way. First, the two components, MMT dispersed in acidulated deionized water and the ODA dissolved in acidulated alcoholic solution, were separately prepared. For the first component, 10 g of MMT was added to 500 g acidulated deionized water containing 25 g of 1 N HCl, and then agitated for 10 hours at 75°C. The resulting colloidal MMT suspension was left for 20 hours to cool to the room temperature, and then was filtered. The MMT particles retained by the filer were dried for 20 hours at 110°C. Meanwhile, 2.5 g ODA was incorporated into a solution consisting of 50 g of isopropyl alcohol (IPA) and 31 g of 1 N HCl, and then continuously stirred until the ODA completely dissolved in this acidulated alcoholic solution, and the solution became transparent. Afterward, 50 g deionized water was added to the ODA solution. Next, 6.7 g of dried MMT (the first component) was added to the ODA solution (the second component), and the mix was vigorously agitated for 5 hours at room temperature to make slurry with suspended MMT particles. The suspension was filtered, and the solid particles remaining on the filter were repeatedly washed with deionized water to eliminate any extra ODA as far as possible, without removing intercalated ones, and then dried for 24 hours at 110°C. The dried ODA-treated MMT mass was pulverized in a vibrating sample mill for use as the filler. A thermoplastic polyphenylenesulfide (PPS) powder with a particle size of < 60 μm was obtained from Ticona. A 45wt% PPS powder was mixed with 55wt% isopropyl alcohol to make a slurry coating. Then, MMT filler at 5, 8, 11, and 14 % by weight of the total

amount of PPS was added to the slurry, and the mix was mechanically blended in a shear blender for 2 min to uniformly disperse the MMT particles throughout the slurry.

The carbon steel coupons were prepared in the following way. First, their surfaces were covered with a zinc phosphate (Zn.Ph) primer by immersing them for 30 min into a phosphate solution consisting of a 5.0 wt% zinc orthophosphate, 10.0 wt% phosphoric acid, 1.0 wt% manganese (II) nitrate hexahydrate, and 84.0 wt% water at 80°C. Then, the Zn.Ph-primed steel surfaces were rinsed with water at 25°C, and dried in an oven at 100°C for 30 min to remove any moisture. The MMT-filled PPS coating systems were deposited on the Zn.Ph-primed coupons as follows. The primed coupons were dipped into the slurry, and withdrawn slowly. The slurry –covered coupons were left for 20 hours at ambient temperatures to volatilize the isopropyl alcohol, and simultaneously, to promote the conversion of the slurry layer into a sintering layer. Then, the sintered layer was heated in air at 310°C for 3 hours to achieve melt flow, and subsequently cooled to room temperature to make a solid film. This coating process was repeated three times more to assemble coating films ranging from 120 to 150 μm thick. The thickness of coating films was determined from cross-sectional examination using scanning electron microscopy (SEM).

Measurements

X-ray diffraction (XRD) was used to determine the shift in position of the basal, d_{001}, peaks for the "as-received" MMT and ODA-treated MMT. Differential scanning calorimetry (DSC) was employed to investigate the changes in melting and crystalline temperatures of the PPS as a function of MMT content. The structures of the untreated and treated MMT-dispersed PPS were explored using transmission electron microscopy (TEM). With Fourier-transform infrared (FT-IR), we investigated the alteration in chemical structure of the PPS containing treated and untreated MMT before and after exposure for 20 days in autoclave containing a CO_2-laden brine solution (0.5wt% sodium hydrogen carbonate,13 wt% sodium chloride, and 86.5 wt% water) at 300°C under a hydrothermal pressure of 8.27 MPa. The coated carbon steel panels (62.5 mm x 62.5 mm) were exposed for up to 20 days in an autoclave containing a CO_2-laden brine solution at 300°C. AC electrochemical impedance spectroscopy (EIS) was used to

evaluate the ability of the exposed coating films to protect the steel from corrosion. The specimens were mounted in a holder, and then inserted into an electrochemical cell. Computer programs were prepared to calculate theoretical impedance spectra and to analyze the experimental data. Specimens with a surface area of 13 cm^2 were exposed to an aerated 0.5 M sodium chloride electrolyte at 25°C, and single-sine technology with an input AC voltage of 10 mV (rms) was employed over a frequency range of 10 KHz to 10^{-2} Hz. To estimate the protective performance of the coatings, the pore resistance, Rp, (ohm-cm^2) was determined from the plateau in Bode-plot scans that occurred in low frequency regions. The results from this EIS test were supported by the analysis of scanning electron microscopy (SEM) images, coupled with energy-dispersive x-ray spectrometry (EDX) of the cross-sectional area of the exposed coating layer. In addition, SEM-EDX was used to identify how well the exposed coating adheres to the ZnPh primer layer.

3. Results and Discussion

ODA-treated MMT/PPS Nanocomposite

Figure 1 depicts the XRD patterns over the diffraction range 2.21 to 0.88 nm for the (a) "as-received" MMT, the (b) ODA-treated MMT, and the (c) ODA-treated MMT-incorporated PPS. The XRD tracing (a) of "as-received" MMT revealed a peak at 1.29 nm, signifying that the opening between the silicate sheets in terms of basal interplanar spacing of MMT is 1.29 nm. When the MMT was treated with the ODA, the XRD pattern (b) showed that the interplanar spacing of MMT had increased to 1.66 nm, while the line intensity at 1.29 nm was strikingly attenuated. Since this increase can be accounted for by the expansion of interplanar spacing, it is reasonable to assume that the ODA, with molecular weight of 269.51, was intercalated in this spacing by ionic exchanges between the Na^+ in the interplanar spaces and $-NH_2^+$ in ODA. After mixing the ODA-intercalated MMT fillers with molten PPS, we observed a considerable decay of the line intensity at 1.66 nm spacing (XRD tracing c). This phenomenon may reflect the co-intercalation of molten PPS in the spacing, followed by the exfoliation of ~ one nm thick silicate sheets. If this interpretation is valid, the nanoscale MMT fillers had became dispersed in the PPS matrix through the processes of ODA intercalation →

molten PPS co-intercalation → exfoliation. Finally, cooling the material led to the formation of the PPS/MMT nanocomposite.

This information was supported by the TEM image analyses (Figure 2). Untreated and ODA-treated MMT-filled PPS solids were cut with a microtome to prepare ~ 100 nm slices for TEM. Figure 2 (left) is a typical TEM image of untreated MMT-filled PPS, revealing the poor dispersion of agglomerated MMT particles in the PPS matrix. In contrast, the image of treated MMT-filled PPS sample (Figure 2, right) highlights well-separated particles of MMT, underscoring that this sample has an exfoliated nanocomposite structure.

Thermal Characterizations

Figure 3 illustrates the cyclic DSC curve of the PPS without MMT that encompasses two endothermic- and one exothermic-transition temperatures. The former endothermic transformations included the glass-transition temperature, T_g, and the melting temperature, T_m. The latter reflected the crystallization temperature, T_c, rendering the exothermic transformation of the molten state of the polymer into a crystal state on cooling. In this curve, our attention focused on investigating the shift in the peak temperatures of T_m and T_c as a function of MMT content.

Figure 4 compares the T_m-related endothermic curves of 0, 5, 8, 11, and 14wt% treated MMT-containing PPS nanocomposites. The bulk PPS noted as "0 %" had a T_m peak of 249°C. This single curve was converted into a doublet curve by adding 5wt% MMT to the PPS; the temperatures of the first and second peaks in this doublet were 255°C and 268°C, respectively. There was a further shift in both the peaks to higher temperature sites after adding 8wt% MMT. With 11wt% MMT, the curve's feature changed again; in particular, the second peak became the principal one, while the heat flow of first peak was strikingly attenuated. A further attenuation and growth of the first and second peaks was seen with 14wt% MMT. Since the first exothermic peak is attributable to the melting point of bulk PPS, it is possible to interpret that the second peak generated at the high temperature site is associated with the melting point of PPS in the nanocomposite structure. Accordingly, the melting point of bulk PPS was

significantly increased by adding MMT; in fact, with 14wt% MMT, it rose by 38°C to 289°C.

Figure 5 shows the changes in DSC exothermic peaks corresponding to the crystalline temperature, T_c, rendering the exothermic transformation of the molten state of PPS into its crystal state on cooling, as a function of MMT content. As seen, the T_c tends to increase as more MMT is incorporated into the PPS. The T_c at 175°C of the bulk PPS without MMT shifted to a high temperature site at 220°C after adding 14wt% MMT to the PPS. Such a shift of T_c seemed to suggest that adding a respectable amount of MMT nanofiller promoted the extent of the melt-cooling crystallization of PPS. To support this interpretation, we determined the heat energy evolved during crystallization from the closed areas of curves with the baseline [15-16]. Figure 6 depicts the changes in crystallization energy of the PPS as a function of MMT content. As seen, the crystallization energy of the bulk PPS was conspicuously enhanced as the 11wt% MMT was added; beyond this content, it decreased somewhat. In exploring the interfaces between crystalable thermoplastic polymers and carbon fiber, several investigators [17-19] reported that the surfaces of carbon fiber preferentially promote the nucleation of the polymer. Correspondingly, the carbon fiber-reinforced polymer had a higher nucleation density than polymer itself. They concluded that the high extent of crystallization of the polymer on the fibers' surfaces was responsible for the development of a strong interfacial bond between them. Relating our findings to these studies, the surfaces of MMT nanofillers with their large aspect ratio provided an abundance of nuclei sites for PPS crystallization. This is the major reason why the crystallization energy of PPS rose with an increasing content of MMT. Conceivably, the excellent adherence of the nanofillers' surfaces to PPS represents good interfacial bonding.

Hydrothermal Oxdation

Figure 7 shows the FT-IR spectra from the 14% MMT-filled PPS nanocomposite film, ~ 0.2 mm thick, before and after exposure for 15 days in autoclave at 300°C. For the former, the spectrum included multiple absorption bands attributed to the two groups, phenyl rings and sulfide linkages, within the PPS, and also to another two groups in the MMT, R(Al, Mg, or Fe)-OH and silicate. The twelve bands at 3064, 3005, 1905, 1645,

1572, 1468, 1389, 1179, 1095, 1079, 1000, and 814 cm^{-1} were associated with the phenyl rings, and the three bands at 743, 670, and 556 cm^{-1} to the sulfide linkages [20, 21]. The remaining two bands at 3630 and 1060 cm^{-1} can be accounted for by the MMT-related groups, the stretching vibration of O-H bond in the R(Al, Mg, or Fe)-OH groups and the stretching modes of the Si-O bond in the silicate groups, respectively [22].

The spectrum of autoclaved film highlights the incorporation of three additional bands at 3470, 1630, and 1232 cm^{-1}. The first two bands were due to the stretching and bending vibrations of H-O-H bond in moisture. According to the literature [23], a possible contributor to new band at 1232 cm^{-1} is the sulfite linkage, -O-SO-O-. Thus, an additional oxygen appears to be incorporated into the PPS film during autoclaving at 300°C, signifying the hydrothermal oxidation of PPS.

To visualize the extent of hydrothermal oxidation of the PPS with and without MMA fillers after autoclaving for 15 days at 300°C, the changes in the absorbance of the –O-SO-O- linkage at 1232 cm^{-1} and the –S- linkage at 670 cm^{-1} as a function of MMT content was investigated (Figure 8). The data revealed that the absorbance of the –O-SO-O- linkage-associated band declined with an increasing content of MMT, while the –S- linkage-related absorbance increased. With 14wt% MMT, the absorbance of the –O-SO-O- linkage was 0.017, which was tantamount to nearly a 1.5-fold decline compared to MMT-free PPS. This finding strongly suggested that the MMT nanofiller inhibited the oxidation of PPS brought about by the attack of 300°C brine.

Corrosion Protection

Our study next shifted to assessing the protection afforded by the PPS/MMT nanocomposite coatings in preventing the corrosion of carbon steel after autoclaving for up to 20 days at 300°C. AC electrochemical impedance spectroscopy (EIS) was used to acquire this information. Figure 9 shows the overall Bode-plot curve of the bulk PPS coating without MMT before exposure. The particular attention was paid to the impedance value in terms of the pore resistance, Rp, which can be determined from the peak in the Bode plot occurring in a low frequency range of 10^{-1} to 10^{-2} Hz. Since the Rp value reflects the magnitude of ionic conductivity generated by a corrosive electrolyte passing through the coating layer, a high Rp value means a low degree of infiltration of

the electrolytes in the coating film, thereby resulting in a good corrosion- preventing performance of coating. Figure 10 plots the changes in Rp of the carbon steel panels (size, 60 mm x 60 mm) coated with 0, 5, 8, 11, and 14wt% MMT-filled PPS materials against exposure times up to 20 days in a CO_2-laden brine at 300°C. Before exposure, the Rp value of all the coated panels ranged from a low of 5.1×10^9 to a high of 9.9×10^9 ohm-cm^2. After exposing the bulk PPS coating panel noted as the "0 % MMT," the Rp value gradually fell, suggesting that extending the exposure time enhanced the rate of uptake of the electrolytes by the coating. A similar decline in the Rp value was observed from the 5wt% MMT/PPS coating. However, the rate was much lower than that of the bulk PPS coating; in fact, the Rp value of 2.6×10^9 ohm-cm^2 for this 20-day exposed coating was nearly 2.7-fold greater than that of the bulk PPS coating at the same exposure time. In contrast, incorporating more than 8wt% of MMT into the PPS impeded the permeation of electrolytes through the coating. There were no significant changes in Rp values for the 20-day exposed 8, 11, and 14wt% MMT-filled coatings, compared with those for these unexposed coatings, demonstrating that a proper amount of MMT nanofillers upgraded the ability of PPS coating to protect the steel against corrosion in 300°C brine environment. However, SEM-EDX exploration of the cross-sectional areas in the 20-day exposed 14wt% MMT coating revealed that some brine had permeated its superficial layer (Figure 11). As is evident from EDX spectrum, a layer extending from the outermost surface to a depth of ~ 25 μm, denoted as area "A", included the brine-related Na element; the other elements, S, Si, Al, O, and C, are derived directly from the PPS and MMT. No Na was detected at the location marked as area "B", that is ~ 50 μm below the surface. With this limited information, there is no clear whether the extent of infiltration of the brine increases with extended exposure times.

One important issue governing the maximum effectiveness of coating in preventing the corrosion of steel is its good adherence to the primer. Poor adherence often causes the generation of blisters where the brine permeates through the coating layers. The ideal mode of adherence is that bond failure at interfaces occurs in either the coating or primer layers. To obtain this information, the 20-day exposed coating layer was removed physically from the Zn.Ph-primed steel surfaces, and then the interfacial site of coating was explored by SEM-EDX to identify the locus of the bond failure at the

interfaces between them (Figure 12). The SEM image revealed that the crystalline Zn.Ph primer layer adhered well to the coating, clearly verifying that interfacial bond failure took place in the Zn.Ph primer layer. This cohesive failure mode can be taken as evidence that the coating was tightly linked to the primer, and also, that the strength of interfacial bond was much greater than that of the primer itself.

Conclusion

The cation- exchange reaction between octadecylamine (ODA) and montomorillonite (MMT) clay led to the intercalation of ODA into the ~ 1.1 nm gallery within the MMT structure. Further, this intercalation played an important role in promoting the exfoliation of individual nanoscale silicate plates formed by the co-intercalation of molten polyphenylensulfide (PPS), thereby generating a nanoscale MMT-filled PPS nanocomposite. Exfoliation not only uniformly dispersed the MMT nanofillers in the PPS matrix, but also conferred three advanced properties on semi-crystalline PPS polymer; 1) an increase in its melting temperature by nearly 40° to ~ 290°C, 2) enhanced crystallization energy, reflecting the development of a good interfacial bond between nanofiller and PPS, and, 3) abatement of its hydrothermal oxidation attributed to the transformation of sulfide → sulfite linkage. When this advanced PPS/MMT nanocomposite was used as the high temperature corrosion-preventing coating of zinc phosphate (Zn.Ph)-primed carbon steel, a coating of ~ 150 μm thickness adequately mitigated corrosion of steel during an exposure for 20 days in a 300°C brine environment. In fact, there were no significant changes in the coating's pore resistance, Rp, that represents the extent of the uptake of corrosive ionic species. In contrast, the Rp value of the coating without MMT declined with increasing exposure time, meaning that prolonging the exposure time enhanced the extent of infiltration of corrosive ionic species through the coating layer. Also, the adherence of the exposed nanocomposite coating to the Zn.Ph primer was outstanding, as verified by the fact that the bond failure at interfaces between the coating and primer took place in the primer layer.

References:

[1] T. Sugama, D. Elling, K. Gawlik, J. Mater. Sci. 37 (2002) 4871.

[2] K. Gawlik, T. Sugama, Geothermal Resources Council Transactions, 24 (2003) 450.

[3] T. Sugama, K. Gawlik, Geothermal Resources Council Transactions, 28 (2004) 365.

[4] T. Sugama, K. Gawlik, Polym. Polym. Compos. 11 (2003) 161.

[5] Y. Komori, K. Kuroda, in: T.J. Pinnavaia and G.W. Beall (Eds.), Polymer-Clay Nanocomposites, John Wiley & Sons, Ltd., New York, 2000, pp. 3-18.

[6] E. Ruiz-Hitzky, P. Aranda, in: T.J. Pinnavaia and G.W. Beall (Eds.), Polymer-Clay Nanocomposites, John Wiley & Sons, Ltd., New York, 2000, pp. 18-46.

[7] C. Chen, D. Curliss, Polym. Materi. Sci. & Eng. 88 (2002) 88.

[8] A. Goldstein, M. Beer, J. Euro. Ceram. Soc. 24 (2004) 3187.

[9] J.Y. Lee, H.K. Lee, Mater. Chem. Phys. 85 (2004) 410.

[10] M. Pospisil, A. Kalendova, P. Capkova, J. Simonik, M. Valaskova, Colloid Interface Sci. 277 (2004) 154.

[11] A.B. Morgan, J.W. Gilman, R.H. Harris, C.L. Jackson, C.A. Wilkie, J. Zhu, Polym. Materi. Sci. & Eng. 83 (2000) 53.

[12] A. Tidjani, C.A. Wilkie, Polym. Degrad. Stab., 74 (2001) 33.

[13] B. Jurkowski, Y.A. Olkhov, Thermochimica Acta, 414 (2004) 243.

[14] C. Lam, H. Cheung, K. Lau, L. Zhou, M. Ho, D. Hui, Composites: Part B, 36 (2005) 263.

[15] C.S. Ray, W. Huang, D.E. Day, J. Am. Ceram. Soc. 74 (1991) 60.

[16] K.F. Kelton, J. Am. Ceram. Soc. 75 (1992) 2449.

[17] A.J. Waddon, M.J. Hill, A. Keller, D.J. Blundell, J. Mater. Sci. 22 (1987) 1773.

[18] X.J. Qian, S.E. Rickert, J.B. Lando, J. Mater. Res. 4 (1989) 1005.

[19] T.Q. Li, M.Q. Zhang, K. Zhang, H.M. Zeng, Polymer, 41 (2000) 161.

[20] R.W. Lenz, C.E. Handlovits, J. Polym. Sci. 53 (1960) 167.

[21] A.B. Port, R.H. Still, J. Appl. Polym. Sci. 24 (1979) 1145.

[22] V.C. Farmer, J.D. Russell, Spectrochimica Acta, 20 (1964) 1149.

[23] L.J. Bellamy, The infrared spectra of complex molecules, Chapman and Hall, London, 1975, pp. 349-410.

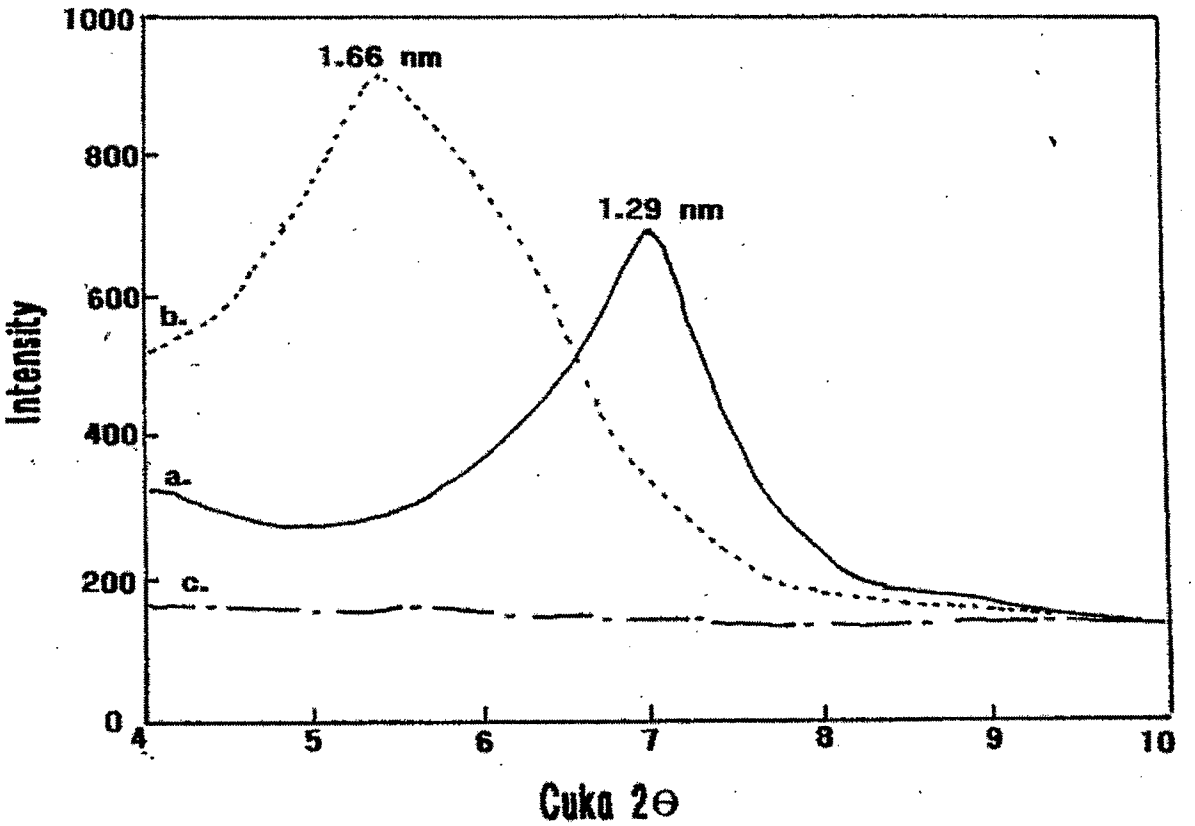

Figure 1. XRD patterns of (a) "as received" MMT, (b) ODA-treated MMT, and, (c) PPS/treated MMT.

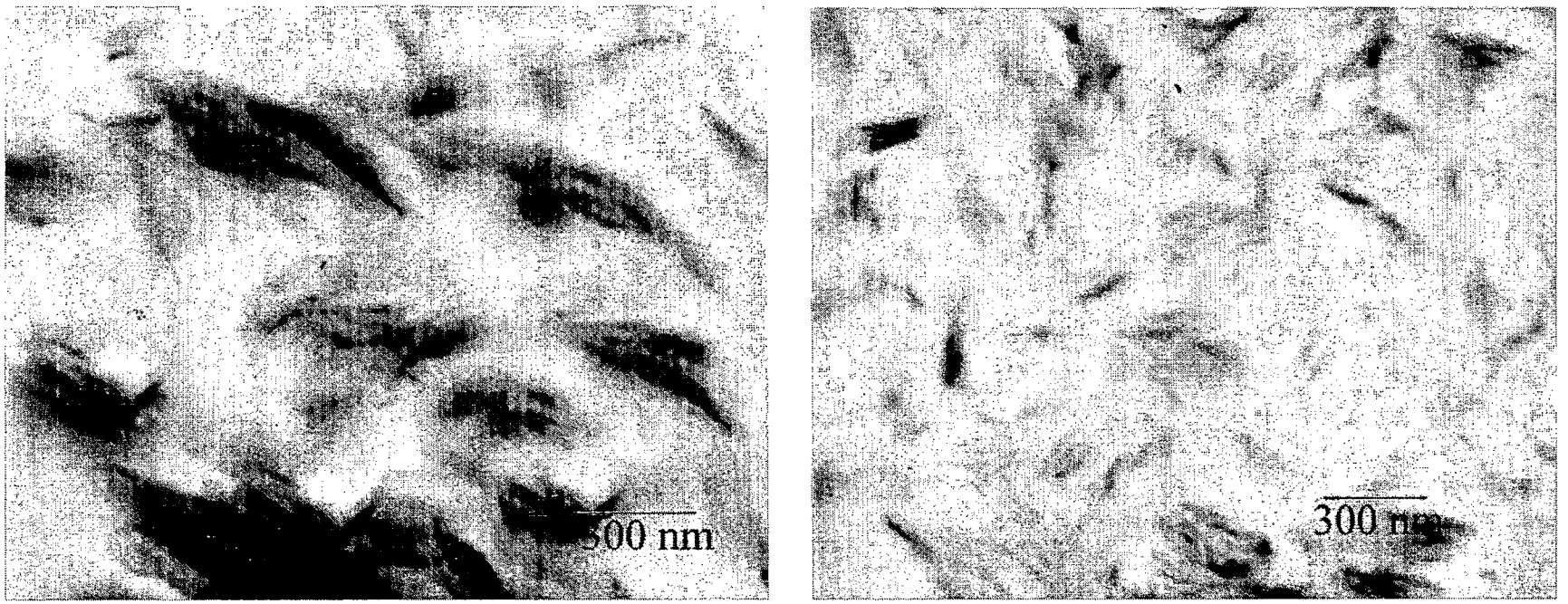

Figure 2. TEM images of untreated MMT/PPS (left) and ODA-treated MMT/PPS (right) systems.

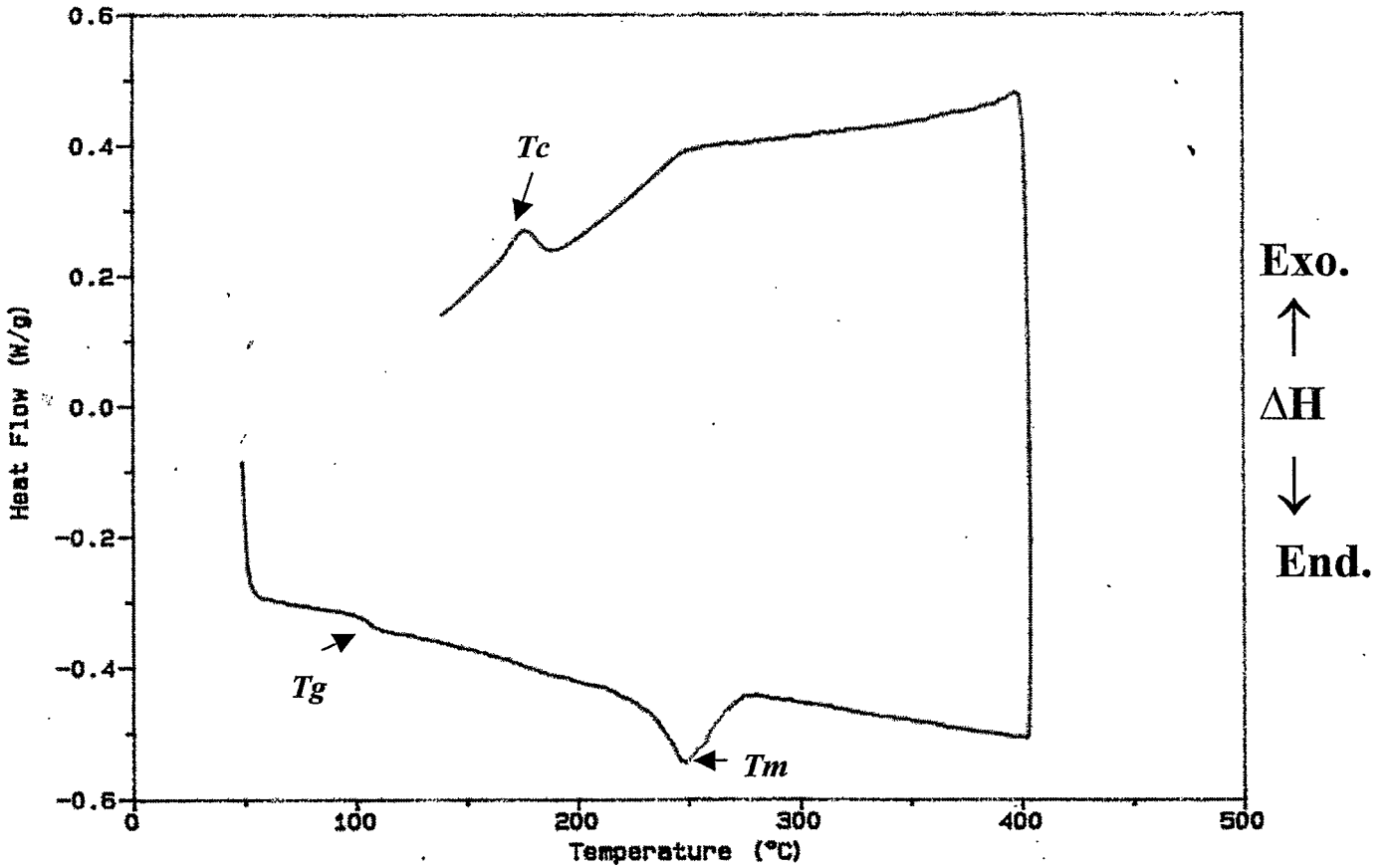

Figure 3. Typical cyclic DSC curve encompassing the glass transition temperature, *Tg,* endothermic melting point, *Tm,* and exothermic crystallization temperature for semi-crystalline PPS.

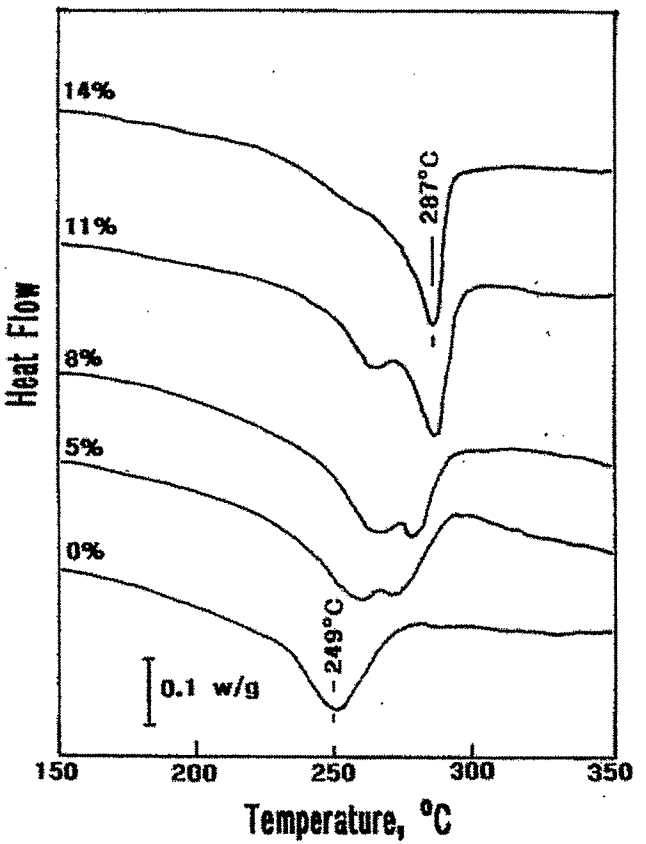

Figure 4. Shift in the melting temperature of PPS as a function of the content of treated MMT.

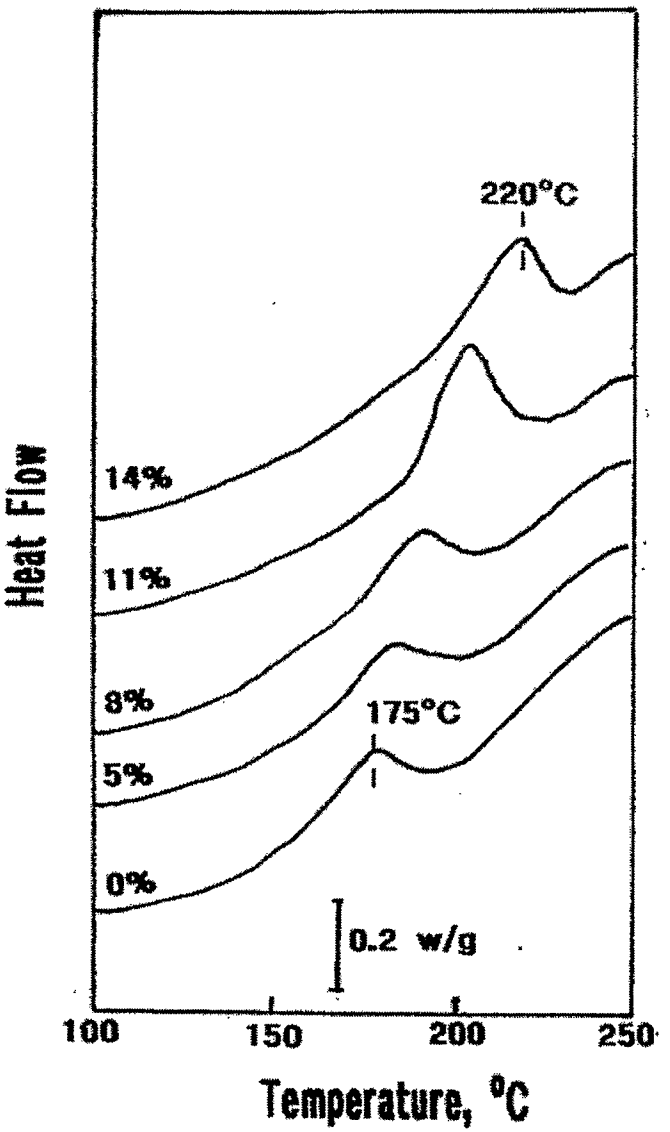

Figure 5. Changes in the exothermic crystallization temperature of PPS as a function of the content of treated MMT.

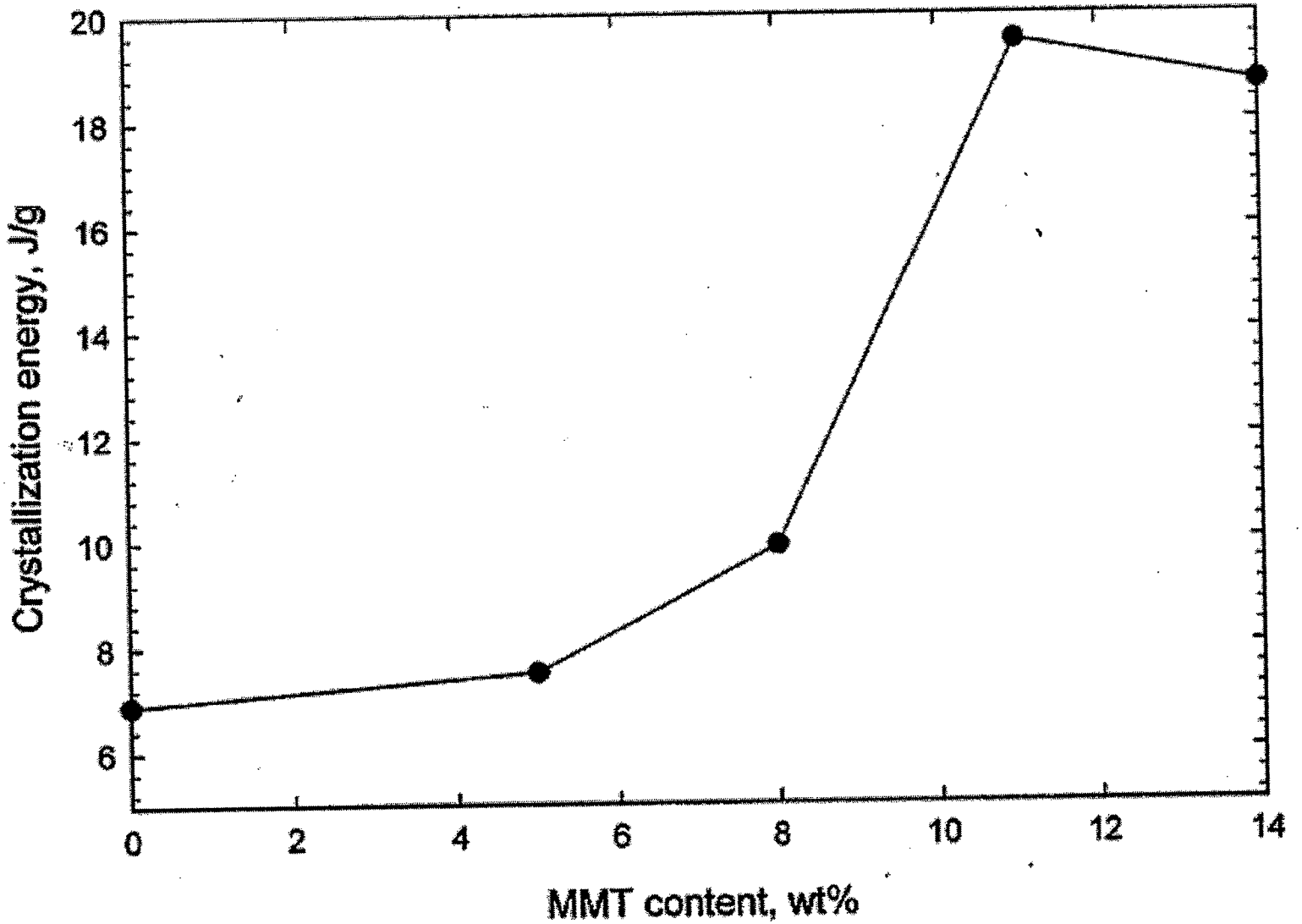

Figure 6. Effect of treated MMT content on the crystallization energy of PPS.

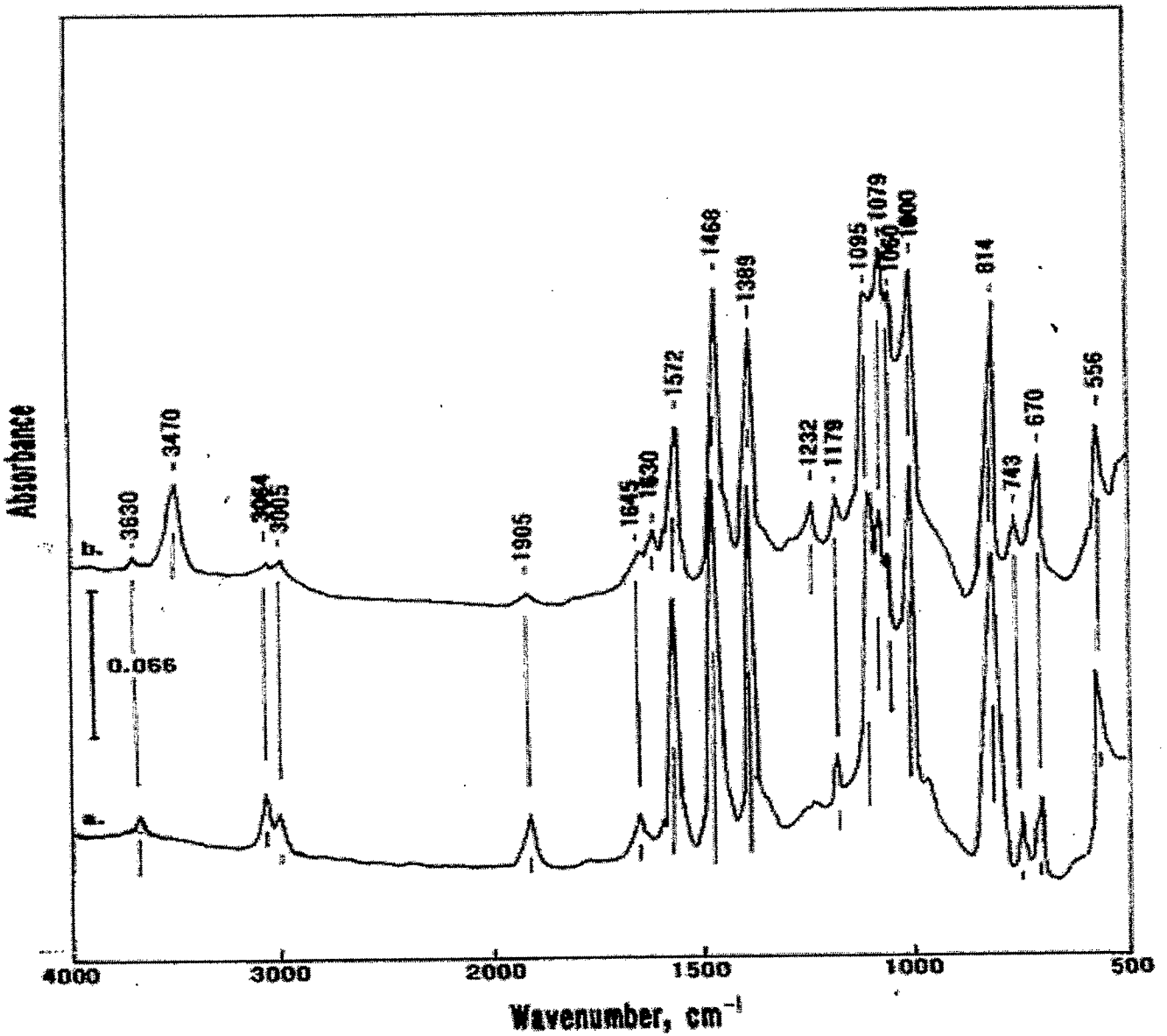

Figure 7. FT-IR spectra for 14% MMT-filled PPS nanocomposite film (a) before, and, (b) after exposure for 15 days in an autoclave at 300°C.

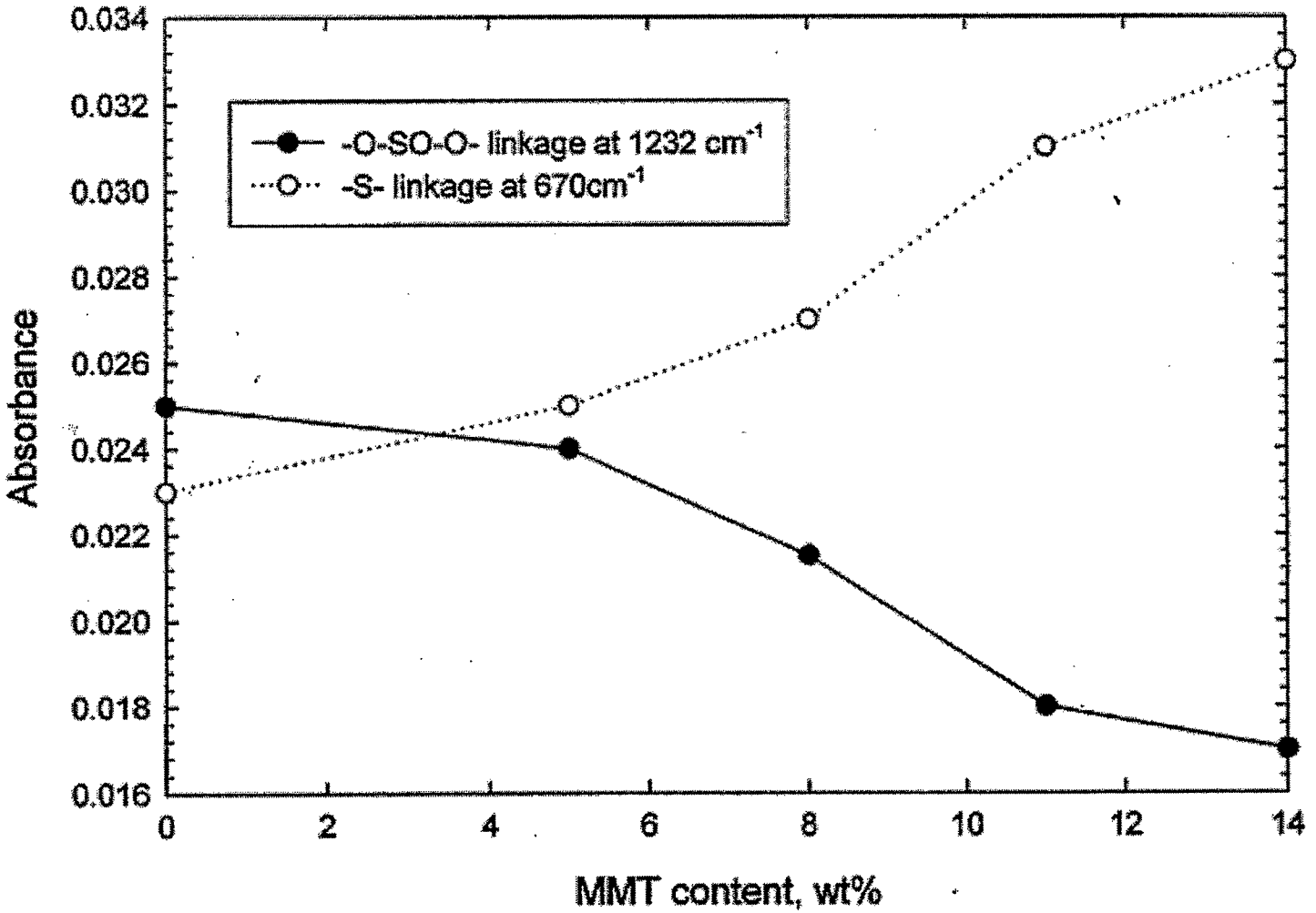

Figure 8. Changes in the absorbance of the sulfide linkage, -S-, at 670 cm^{-1} and the sulfite linkage, -O-SO-O-, at 1232 cm^{-1}as a function of the content of treated MMT.

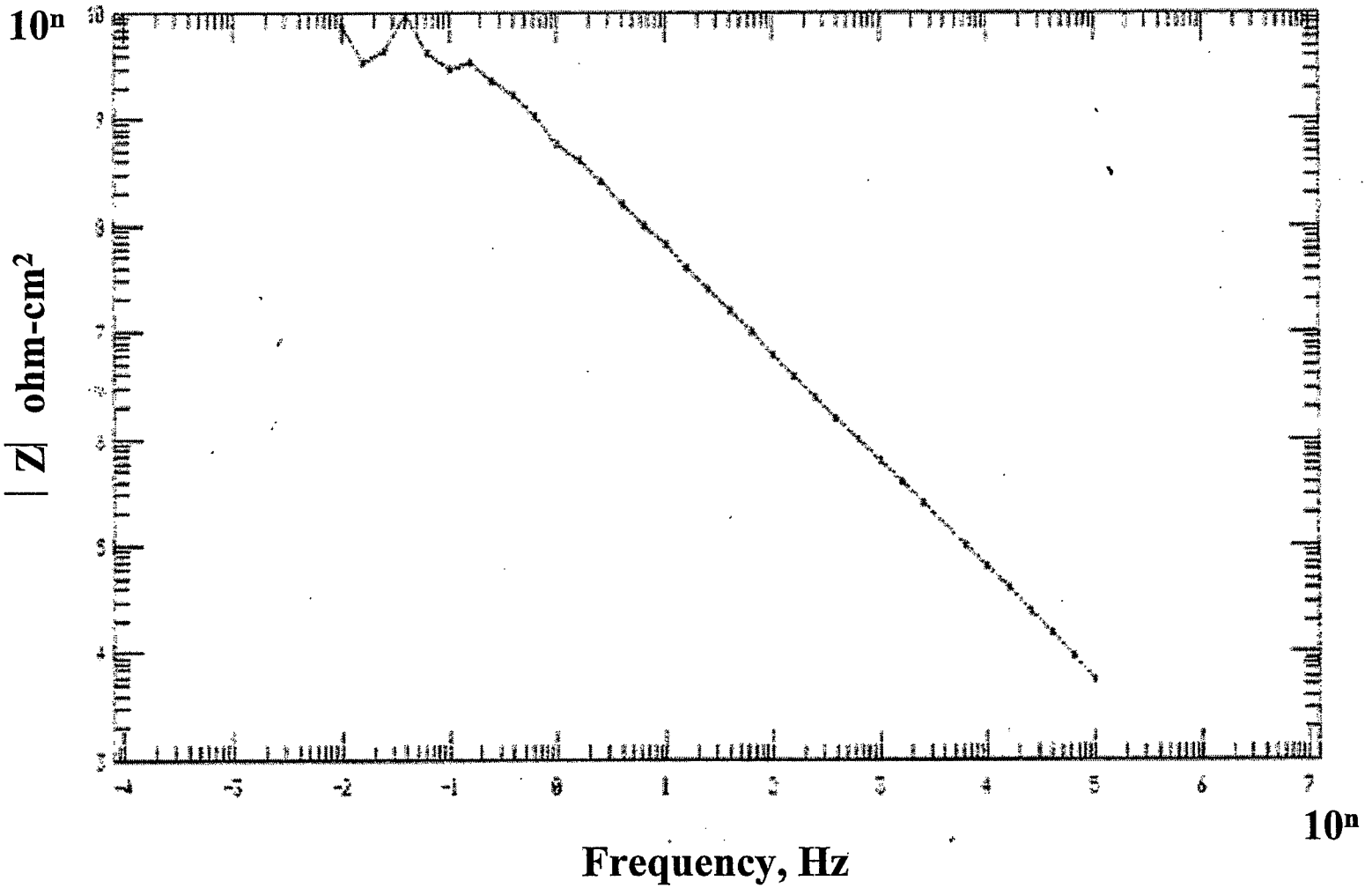

Figure 9. Bode-plot curve of the bulk PPS coating without MMT before exposure.

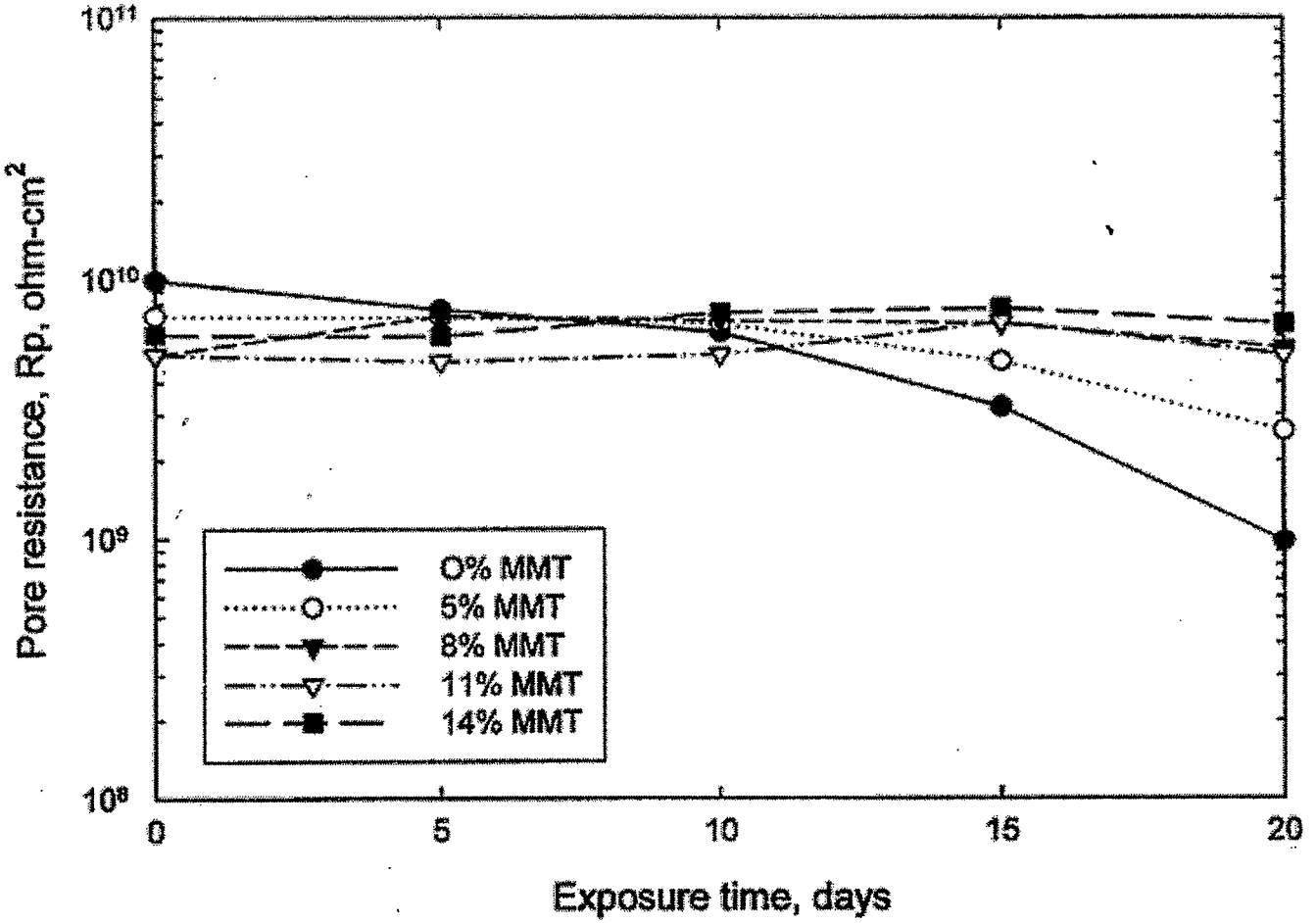

Figure 10. Pore resistance, Rp, of the PPS coatings containing 0, 5, 8, 11, and 14 wt% treated MMT after exposure for up to 20 days in a 300°C brine.

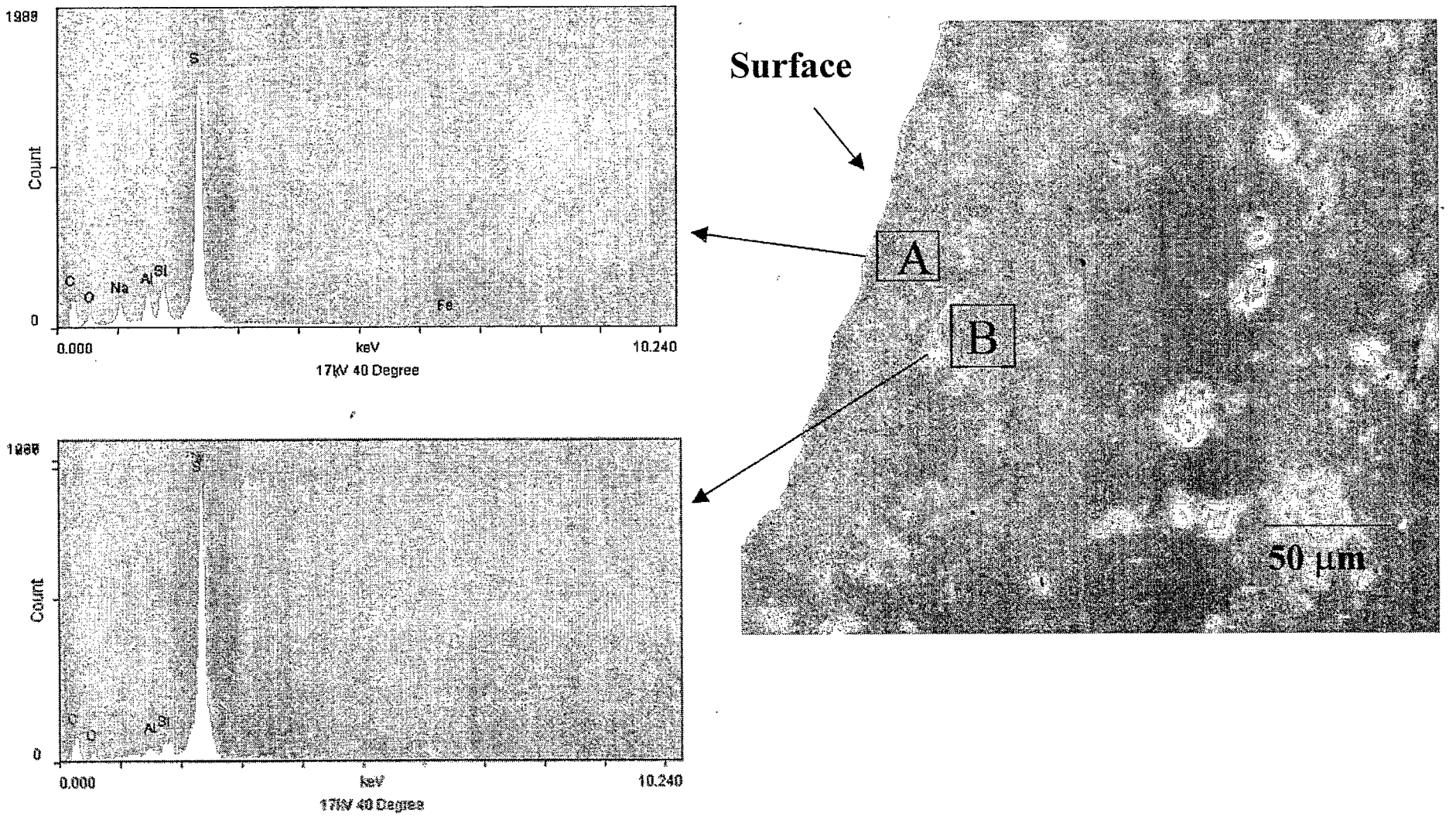

Figure 11. SEM image coupled with EDX spectra of a cross-sectional area of a 20-day-exposed 14wt% MMT/PPS nanocomposite coating layer deposited on the carbon steel's surface.

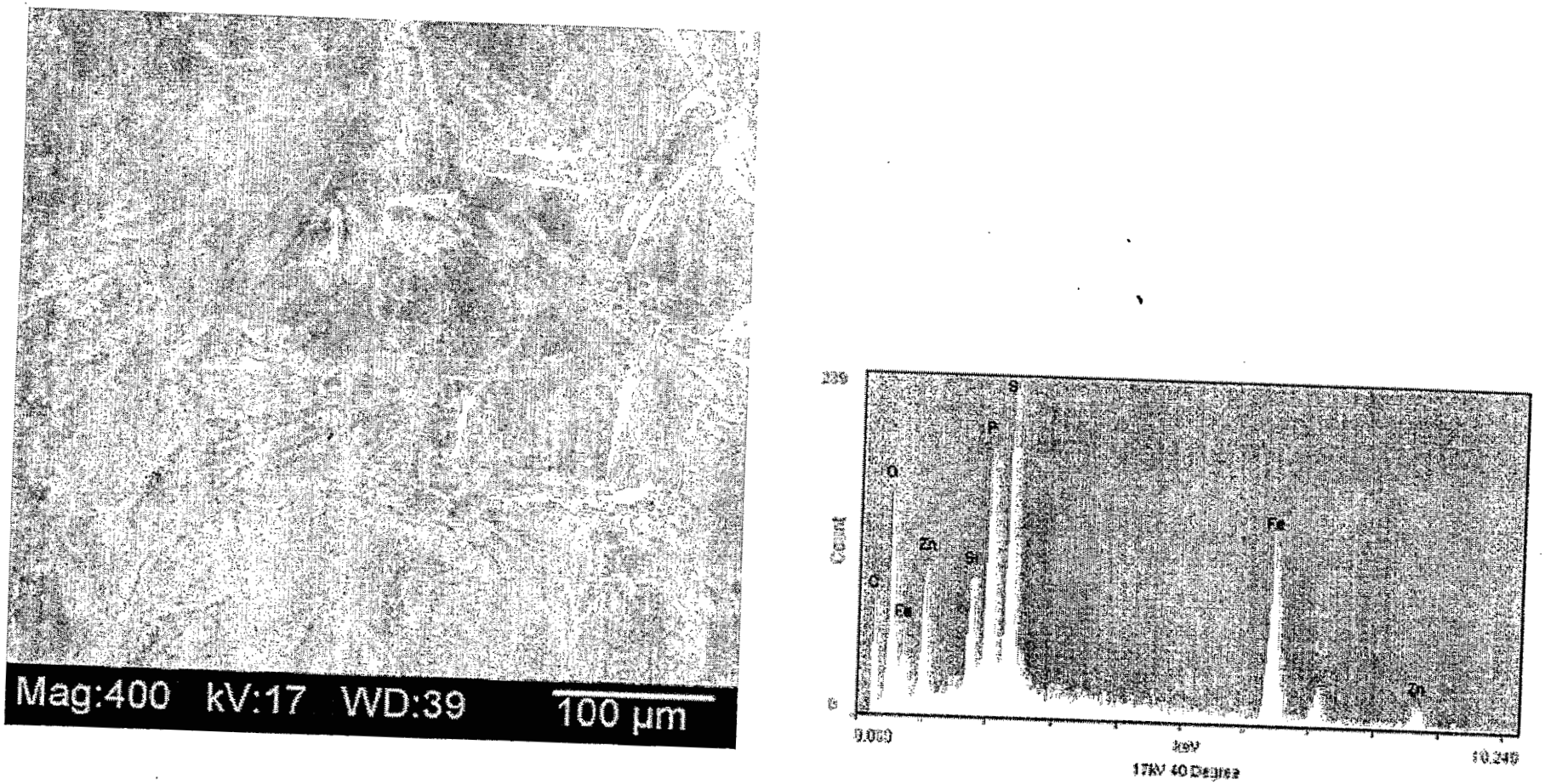

Figure 12. SEM-EDX exploration of the interfacial coating site peeled off from the zinc phosphate-primed steel's surface.